

## A computational workflow to analyse material properties and solar radiation of existing contexts from attribute information of point cloud data

Alkadri, Miktha; Turrin, Michela; Sariyildiz, Sevil

**DOI**

[10.1016/j.buildenv.2019.03.057](https://doi.org/10.1016/j.buildenv.2019.03.057)

**Publication date**

2019

**Document Version**

Final published version

**Published in**

Building and Environment

**Citation (APA)**

Alkadri, M., Turrin, M., & Sariyildiz, S. (2019). A computational workflow to analyse material properties and solar radiation of existing contexts from attribute information of point cloud data. *Building and Environment*, 155, 268-282. <https://doi.org/10.1016/j.buildenv.2019.03.057>

**Important note**

To cite this publication, please use the final published version (if applicable). Please check the document version above.

**Copyright**

Other than for strictly personal use, it is not permitted to download, forward or distribute the text or part of it, without the consent of the author(s) and/or copyright holder(s), unless the work is under an open content license such as Creative Commons.

**Takedown policy**

Please contact us and provide details if you believe this document breaches copyrights. We will remove access to the work immediately and investigate your claim.

***Green Open Access added to TU Delft Institutional Repository***

***'You share, we take care!' - Taverne project***

**<https://www.openaccess.nl/en/you-share-we-take-care>**

Otherwise as indicated in the copyright section: the publisher is the copyright holder of this work and the author uses the Dutch legislation to make this work public.



# A computational workflow to analyse material properties and solar radiation of existing contexts from attribute information of point cloud data

Miktha Farid Alkadri\*, Michela Turrin, Sevil Sariyildiz

Chair of Design Informatics, Faculty of Architecture and the Built Environment, Delft University of Technology, Julianalaan 134, 2628BL, Delft, the Netherlands

## ARTICLE INFO

### Keywords:

Site analysis  
Point cloud data  
Attribute information  
Material properties  
Solar radiation

## ABSTRACT

This paper investigates a prospective application of point cloud data in supporting the contextual analysis of the built environment during the conceptual design process. Often, the complexity of site information causes architects to neglect several relevant properties that may affect environmental performance analysis, especially when dealing with a complex design case. For example, the current approaches of 3D site modelling lack an understanding of the site characteristics of existing environments with respect to either geometrical or material properties. With the advancement of 3D laser scanning technologies, capturing complex information from real contexts offers great possibilities for architects. From geometric and radiometric information stored within point cloud data, this study specifically proposes a novel approach to contextual analysis that considers material aspects and simulates solar radiation in the real environment. In doing so, three computational stages are developed. First, the correction of a raw dataset is designed to not only minimize errors during the scanning process but to also clean the selected dataset. Second, material exploration and the simulation of solar radiation are respectively used to calculate material properties and solar energy in the existing built environment. Third, an integrated environmental simulation aims at identifying materials found in existing areas within a certain level of insolation. As a form of design decision-making support, the present study ultimately generates a computational workflow for analysing the built environment from which architects may conduct a comprehensive analysis of an existing context before initiating design exploration.

## 1. Introduction

The conceptual design stage is of the utmost importance to produce the most significant decision of architectural design process [1]. Within this stage, contextual analysis plays a prominent role in identifying relevant information for design input. Architects should be able to measure the environmental impacts of the proposed design to maintain the quality of the existing context. However, due to the complexity of information related to a building site, understanding the characteristics of the existing context comprehensively remains a great challenge when dealing with a complex design case. In most cases, existing approaches to 3D site modelling (e.g., solid modelling [2,3]) pose several barriers that may result in the following features missing from the contextual analysis:

- The complex geometry of the existing context is not considered, especially when dealing with isolated and dense areas [4]. Consequently, it will often take too much time for modelling construction to consider detailed site properties.

- Building-focused contexts tend to be explored, which consequently neglects surrounding properties such as vegetation or other temporal site elements [5,6]. This matters when conducting environmental simulations of processes such as the UHI (urban heat island) effect or when addressing microclimatic issues.
- Material characteristics of the existing environment [7,8] have yet to be considered properly in 3D site modelling. This can greatly affect the calculation of environmental impacts for both proposed and existing buildings. In conventional design processes, material studies are frequently paid less attention to during the form generation process, and most of the material attributes geometrically applies when adapting architectural components (e.g., concrete for walls or ceramic tiles for flooring) [9,10]. Consequently, it will be challenging to identify different material properties within a single component due to the use of fixed materials. As a matter of the fact, such material properties will be extremely likely to present the same values for different architectural components due to being positioned within the same environmental settings.

\* Corresponding author.

E-mail addresses: [M.F.Alkadri@tudelft.nl](mailto:M.F.Alkadri@tudelft.nl) (M.F. Alkadri), [M.Turrin@tudelft.nl](mailto:M.Turrin@tudelft.nl) (M. Turrin), [I.S.Sariyildiz@tudelft.nl](mailto:I.S.Sariyildiz@tudelft.nl) (S. Sariyildiz).

On the other hand, the advancement of 3D laser scanning technologies has enabled one to easily capture complex information from real contexts. A potential application of point cloud data may include making information relevant to the aforementioned gaps available. In this case, a point cloud consists of geometric and radiometric information [11,12] or may refer to visible and invisible properties, respectively. Visible properties are stored in a colour point cloud, which geometrically represents a real 3D model of the existing environment. Meanwhile, invisible properties include attribute or metadata information associated with each record of measurement [13]. On the basis of point cloud data, this study proposes an approach to environmental performance analysis that involves an integrated workflow of material studies and the solar simulation of an existing context. The present investigation of material aspects aims at mapping surface properties of the existing environment with the support of radiometric information while geometric information may cater to the simulation task of solar radiation. With this integration, the novel method proposed in this work makes several contributions to the current workflow of the architectural design process:

- The attribute information of point cloud data (position-XYZ, colour-RGB, and reflection intensity-I) allows one to easily conduct an environmental analysis during the conceptual design phase, especially in regard to the material performance of existing environments. After investigating optical and thermal properties, a surface distribution catalogue can be generated to identify the material characteristics of existing areas. This can be helpful to architects wishing to perform comprehensive site analysis before making a design decision.
- A point cloud-based solar simulation can effectively mitigate geometric concerns related to the 3D modelling context. Relative to the existing approach, the solar simulation method can be performed without necessarily converting a complex dataset of point clouds into a massive 3D mesh model. This process can be used to identify further opportunities to run more environmental simulations directly based on an unstructured point cloud dataset. The inclusion of more site properties during a simulation may also enrich environmental simulation results.
- Integration between a material database and insolation values allows one to measure the specific performance of any surface within an existing dataset. Accordingly, architects are presented with a fully informed site database that can be used to identify vulnerable areas that may affect the performance of the proposed design. In this case, architects not only need to balance the geometrical relationship between surrounding buildings and the proposed design but must also balance surface materials (performance of the building skin) between them.

This work is divided into several sections. Section 1 presents an overview of the study, describing information missing from current architectural design approaches and following with a note on the relevance of point cloud data for addressing the highlighted issues emerging during site analysis. Section 2 presents a theoretical background that specifically investigates potential applications of point cloud data to material properties, and solar radiation analysis. An in-depth discussion of computational design methods is then given in Section 3. Our dataset collection approach and a detailed analysis of our findings are given in Sections 4 and 5, respectively. Finally, Section 6 presents a conclusion and recommendations for future study.

## 2. Theoretical background

As a facet of design decision-making support, we principally attempt to perform a contextual analysis taking into account the real environment. In doing so, point cloud data are used to provide relevant information in support of the two primary subjects of this study: material

properties and solar radiation analysis. Raw dataset correction is also briefly discussed as a guide to dataset preparation before processing the next stage. The present section will describe specific features of these subjects through the following discussion.

### 2.1. Point cloud data

#### 2.1.1. Geometric information

As a product of laser technology, point clouds have been widely implemented in many fields such as building construction [14–16], landscape modelling [17,18], cultural heritage [19–21] and environmental engineering [22–24]. Weinmann [25] describes a point cloud as having two parts: the “point” geometrically speaking represents the particular unit of location in a specific space and the “cloud” refers to the unorganized arrangement within a blurred spatial boundary. Otepka et al. [26]. define a point cloud as a set of points that are attached to three-dimensional Cartesian space. As an extension of these definitions, Randall [27] exemplifies several particular functions of the geometric information of point cloud data as follows:

- To draw the position of an object with 3D coordinates in a global coordinate system.
- To illustrate geometrical features such as the length between two points and the orientation of objects.
- To illustrate visual information such as 2D and 3D digital images and 3D virtual models.
- To support physical features such as textures, cracks and different types of objects of varying density [28].

These functions, furthermore, create an opportunity to not only cater to data visualization but to also drive precise simulation performance [29]. For example, with the support of 3D colour point cloud data, some existing studies of archaeology and heritage [30,31] have successfully investigated the geometric aspects of building materials. However, these material studies are predominantly performed on the basis of the massive 3D mesh model. This approach, unfortunately, presents several important issues, including the means of reconstructing point cloud data to a 3D mesh model, which consumes large volumes of computational storage, and the scale of the 3D mesh model for archaeology, which primarily deals with smaller objects than those of architectural building or urban scales. Thus, it is critical to develop an efficient method that can handle the dataset processing of architectural contexts without compromising the quality of performance analysis.

#### 2.1.2. Radiometric information

The entity of radiometric information refers to attribute properties of each point within a dataset. Richter [32] notes six values of attribute information that can be further investigated to provide an accurate representation of a point cloud: colour [33], object class information consisting of vegetation [34] and terrain [35], surface normal [36], horizontality [37], and global and local height [38]. However, only a few attributes are practically relevant during architectural design practice. The issue is not rooted in mere design objectives; rather, it originates from the prerequisites of particular attributes. Prior knowledge and pre-processing steps are still needed to extract the full functions of information properties. It is necessary, therefore, for architects to identify the feasibility of using attribute information that fits into the domain of a design framework.

To examine the context of environmental performance analysis in greater detail, this study focuses on the exploration of typical attributes of point cloud data, including coordinate positions (XYZ), colour information (RGB), and reflection intensity (I) [39–41]. Each of these attributes supports different tasks. For example, colour information is used to extract a certain area or object according to its colour values. This possibility can be observed during the identification of road signage by converting RGB colour into HSV values [33]. Similarly,

Ochmann et al. [42] examine colour and surface normal attributes to identify the inner surfaces of room volumes. Meanwhile, the reflection intensity constitutes the return strength value of the laser pulse of each recorded point, which represents degree of reflectivity measured from scanned objects [43]. In other words, intensity values rely heavily on the surface properties and materials of scanned objects [44]. Practical implementation can involve the detection of damaged concrete in a tunnel, pavement lines or stripping; the mapping of the seafloor, and the mapping of geological layers and damage caused by a natural disaster [12]. Furthermore, position information serves as an index of the coordinate location of each point that automatically aligns to both colour and intensity values of a dataset. For this reason, it is feasible to select certain areas of the dataset according to its attached values.

The attributes mentioned above explicitly facilitate the extension of the particular performance of point cloud data, to not only facilitate impressive 3D visualizations but to also drive environmental analysis during the conceptual design stage. When it comes to the site analysis process, these attributes may be able to enhance the sensitivity of site investigations, especially of those dealing with microclimatic issues affecting a dense area.

## 2.2. Correction of the raw dataset

As end-users of 3D scanning technology, architects are responsible for not only understanding relevant information from a dataset but for also identifying factors that may affect a dataset during scanning such as environmental conditions, meteorological conditions, atmospheric pollution [45,46], scanner mechanisms, object properties, and scanning geometries [47]. In this case, point cloud data usually present technical issues related to dataset transformation and computational processing. For example, the TLS (terrestrial laser scanner) dataset often consists of a highly dense dataset such that it must be employed using a powerful workstation [48], and the interoperability the dataset results due to the use of different formats, quality levels and units among default scanners [49]. Such aspects must therefore be managed beforehand to allow for dataset processing.

After establishing the selected dataset, the correction of a raw dataset involves intensity correction. This aims at examining nearly “true” values of intensity as a means preventing erroneous measurements from being made during scanning (e.g., sensor noise, hardware sensitivity, laser wavelengths, and the surface geometry of the target) [50,51]. In addition, Kashani et al. [12] specifically describe several parameters that influence intensity values of a raw dataset such as target surface characteristics, acquisition geometries, and instrumental and environmental effects. These factors, however, cannot be fully compensated for due to local constraints such as atmospheric conditions (humidity and temperature pressure levels) and default features from the manufacturer. Consequently, manual adjustment will still be required even though this is challenging for common users such as architects.

This study specifically applies an intensity correction to a raw dataset by focusing on the acquisition geometry from the angle of incident ( $\alpha$ ). The angle of incident is the angle between the surface normal vector and incident radiation vector [52,53]. One can be observed from the oblique surface of a building that produces more backscattering cross-sections than a direct surface when struck with a laser beam [12]. As the TLS dataset largely depends on the tools and manufacturers of laser scanners [52], distance effects are not considered further in this case. The distance between the instrument's position and scanned areas also adheres to a tolerated distance between the brightness-reducer and scanner.

## 2.3. Material properties

In the preliminary design stage, a crucial task facing architects is to identify environmental impacts on the existing context that may affect a new building and vice versa. In relation to this, the potential

application of point cloud data progressively enables one to investigate materials in the existing environment. Some publications have attempted to address surface material properties by making use of RGB colour and intensity values taken from TLS datasets. Some of these studies perform non-invasive material analysis through the measurement of chemical properties and from the albedo of scanned objects [54], and investigations of reflecting surface properties based on effects on the maximum range and the range delay error [55], and based on different surface conditions (e.g., wetness and darkness) [56–58]. Material properties can also be found from LIDAR (light detection and ranging) datasets through the BRDF (bidirectional reflectance distribution function) model and intensity data [59], and through the use of lidar return density values in identifying water bodies [60]. The objectives of these works, however, predominantly focus on the geometric accuracy of surface characteristics (roughness and reflectance) of different material samples determined from indoor laboratory experiments while in this study material properties are investigated by taking into account both optical and thermal properties according to a dataset of a real building context. Moreover, we perform intensity corrections on a raw dataset to compensate for factors related to data acquisition geometries, which are mostly absent from the existing material studies of TLS datasets.

Furthermore, Kigle-Boeckler [61] describes four key elements in defining surface properties of objects, including materials (e.g., coating, plastic, or metal), surface topographies (e.g., smooth, rough, or structured), the degree of transparency, and the substrate. Based on these items, the present study examines surface materials of a real building dataset by focusing on two aspects: thermal and optical properties.

First, thermal properties demonstrate the quality or attributes of a material, which shape the response process when dealing with the conductivity of heat or with heat fluctuations over time [62]. For the dataset of a point cloud, the following indicators are measured to facilitate the identification of surface materials.

### 2.3.1. Albedo

Albedo refers to the fraction of sunlight reflected from a material or surface [63–65]. Albedo values have a significant impact related on the energy balance of an urban environment, as they constitute absorbance percentages of solar energy. As such, albedo can be used to describe the environmental characteristics of certain areas. Albedo values range between 0 and 1 where a lower value corresponds to a blackbody [66].

### 2.3.2. Emissivity

According to Ashby et al. [67], emissivity refers to heat radiation emitted by the surface of a material. It is also defined as the ratio of radiated light reflected from a material to the volume emitted to a blackbody for the same temperature, wavelength, and emission direction [68]. In contrast to emissivity data, intensity information of point cloud data takes a value of 1.0 for a bright (white) surface or perfect reflector while a perfect emitter (black) is assigned a value of 0. Examples include materials with smooth and shiny surfaces such as plastics, ceramics, water and polished metals, which are generally characterized by high-intensity values but low levels of emissivity [69]. While in principle both emissivity and intensity determine their values contrarily, they consider a similar aspect related to the material of the object's surface. In so doing, the determination of emissivity values can be identified from corrected intensity information.

Second, materials with optical properties are principally determined through their interactions with light or electromagnetic radiation. Regarding optical properties this study focuses on investigating reflectivity and translucent values of materials by taking into account the RGB colour of each point within a dataset. Section 3.1 presents a detailed calculation of these values.

### 2.3.3. Reflectivity

In general, reflectivity describes the amount of light reflected from a

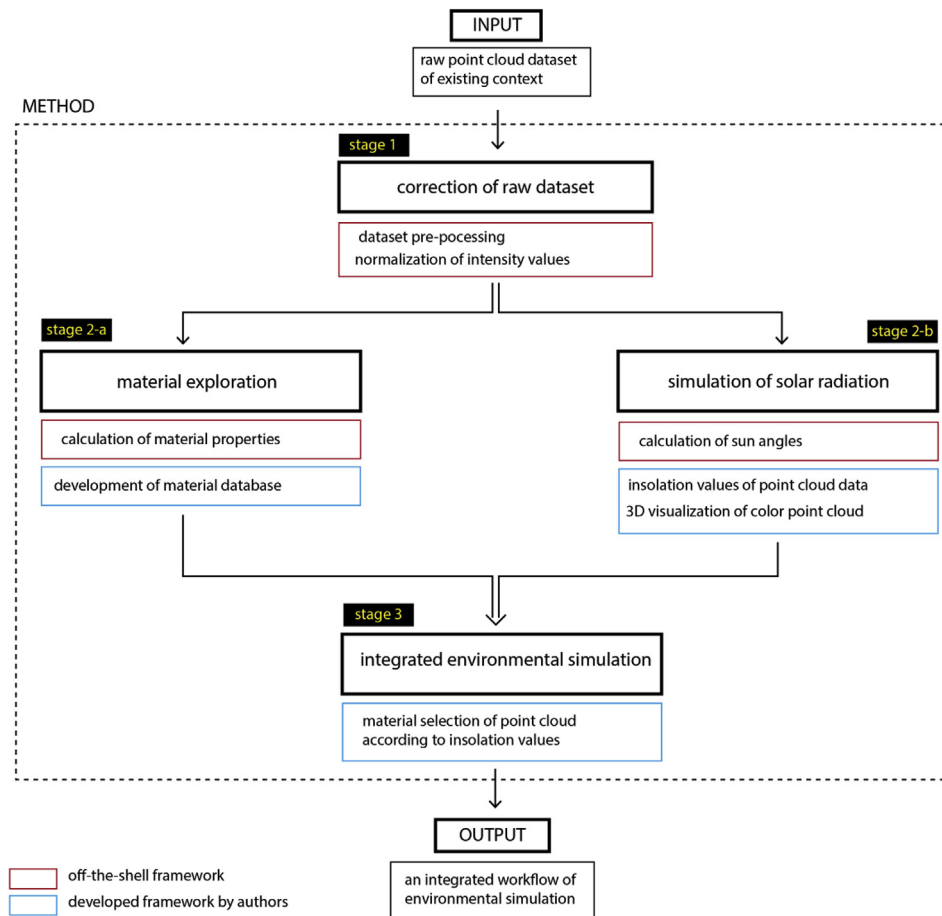


Fig. 1. Overview of the computational workflow.

material in relation to the total amount of incident light that reaches the surface of a material [67,68]. Marsh [70] furthermore distinguishes reflectivity from reflectance. As a boundary property, reflectivity refers to a layer between two particular types of objects while reflectance corresponds to a layer between two specific instances of objects. Nevertheless, in the case of opaque materials, both reflectivity and reflectance are of equal value except in the case of transparent objects, as internal reflections within such materials appear to have a considerable effect. In accordance with a given point cloud dataset, the calculation of reflectivity values in this study predominantly covers opaque materials due to laser scanning capacities. With current applications of laser scanning, a fully transparent record of objects results in a coarse cloud of points within a dataset. This simultaneously confirms the scope of this study on reflectivity properties.

#### 2.3.4. Translucency

An investigation of translucent properties of a material inevitably also involves the calculation of its transmittance values. Transmittance is a material property reflecting a material's capacity to transmit light received through the material itself [70]. In turn, opaque materials should present a zero transmittance value as they cannot be penetrated by light. In regard to a point cloud dataset, one can calculate transmittance values of materials from colour information for each point. Following from this assumption, as long as a dataset contains RGB colour, the translucence of materials can be identified in parallel with a comparison of its reflectance values. Such a calculation is also supported through material mapping with ElumTools [71] when transmittance values are added to opaque material properties, allowing the selected objects to be categorized into a translucent material.

#### 2.4. Solar radiation analysis

An insolation analysis involves evaluating how building surfaces absorb thermal energy from the sun [72]. During conceptual design, evaluating the relationship between a building and the sun is critical to ensuring the behavioral performance of buildings based on optimal sunlight conditions. This process ultimately becomes relevant not only for a proposed building but it can also be extended to existing buildings through contextual analysis. For example, the simulation of solar radiation allows us to map the average solar energy of each panel on a building's façade. In turn, the potential amount of solar radiation reaching a building or site surfaces can be identified and further analysed.

However, as the issue that matters most for current simulation approaches to solar radiation, the 3D digital model of the existing context is primarily constructed by means of basic architectural geometric shapes. In regard to surface characteristics of buildings, the exclusion of textures from the context model and of other relevant site properties can considerably affect the interpretation of simulation results [73]. Things become even more complex when dealing with the 3D model for an isolated context or urban scale forms. Horvat and Dubois [74] reveal that less than 10% of architects are satisfied with the utilization of various solar simulation tools. It is thus, important to at least consider surface properties of the existing environment during the simulation of solar radiation.

In the meantime, some existing works have conducted solar radiation analysis by making use of point cloud data. For example, in using a LiDAR DEM (digital elevation modelling) dataset, Kassner et al. [23] attempted to identify areas of high solar potential on a building's roof and the suitability of a PV (photovoltaic) system for urban areas by

means of pyranometer measurements [75]. Carneiro et al. [24] and Jochem et al. [76] develop solar radiation models in urban areas to deliver an automated solar potential assessment. Similarly, an interactive 3D visualization of the solar urban model [77] has been generated to calculate the solar irradiance distribution based on roof and building facades [78]. Later, Pavlovski et al. [79] from a solar resource campus map and Li et al. [80] in using a pixel-based approach quantify solar energy stored within an existing building's roof and infrastructures. As a major concern related to these approaches, their workflows are inclined towards the domain of environmental engineering, which predominantly uses ALS (Airborne LiDAR) datasets. Meanwhile, studies have yet to focus on the use of TLS datasets rather than ALS datasets due to accuracy concerns [81,82], high-resolution formats [27,83], and broader coverage of isolated areas. Moreover, integration with the architectural design process has yet to be addressed and particularly in relation to site analysis based on TLS datasets. The present study ultimately attempts to address these issues by proposing a computational design method in the following section.

### 3. Development of the computational design method

As introduced in the previous section, the ultimate goal of this study is to develop an integrated workflow of environmental performance analysis for material studies and solar simulations by taking into account point cloud data for the existing environment. A series of computational procedures is developed to support this goal (see Fig. 1); this involves the use of existing frameworks such as point cloud dataset processing and the normalization of intensity values in a first stage and then calculating material properties and sun angles in a second stage. In line with this, several specific frameworks are developed by the authors, including material database formation and the calculation of insolation values of point cloud data in a second stage and the material selection of point clouds based on insolation values in a third stage.

To illustrate the proposed workflow, a detailed discussion of inputs, procedures, digital tools, and outputs of each stage are addressed below.

#### 3.1. Correction of the raw dataset

As noted in Section 2.2, in this study we perform raw dataset corrections. This process mainly involves two tasks: pre-processing and intensity correction. Fig. 2 presents a detailed account of this stage.

Before the dataset is readily used for architectural design analysis, several preliminary steps are completed to avoid irrelevant properties that may compromise workflow performance. These steps involve noise reduction and outlier (unnecessary clouds of points) removal, the selection of attribute order and dataset formats due to interoperability issues emerging during analysis, and the activation of scalar field functions to identify metadata information for a point cloud. These preliminary tasks are computationally supported by Cloud Compare (CC) [84]. One task involves reducing the density of points to manage computation time and calculation requirements of the dataset.

For intensity corrections ( $I_c$ ), we use the following equation [12].

$$I_c = I_{raw} \cdot \frac{1}{\cos \alpha} \quad (1)$$

where  $I_c$  = corrected intensity

$I_{raw}$  = original intensity  
 $\alpha$  = angle of incidence

The angle of incidence is determined with equation [50] below based on the assumption that the initial positioning of the laser scanner is known at (0,0,0).

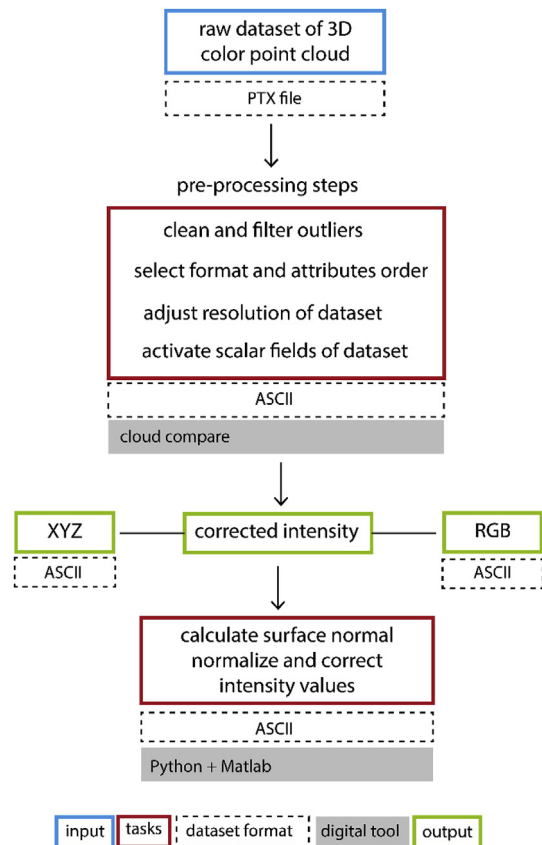


Fig. 2. Correction of the raw dataset.

$$i = \cos^{-1} \left( \frac{\overline{dn} \cdot \overline{dl}}{|\overline{dn}| |\overline{dl}|} \right) \quad (2)$$

where  $i$  = incident angle ( $\alpha$ )

$\overline{dn}$  = direction of surface normal  
 $\overline{dl}$  = direction of the laser pulse

Before applying these algorithmic functions for intensity corrections, the raw intensity values must first be normalized. This procedure is designed to calibrate the numerical index of the original dataset during arithmetic operation.

#### 3.1.1. Material exploration

This stage involves two main steps (see Fig. 3): *first*, material properties (thermal and optical properties) derived from attribute information such as XYZ, RGB, and corrected intensity values are calculated, and *second*, a material database derived from the calculation of material properties is developed. Material selection can then be performed with the material database according to the established criteria.

As described in Section 2, thermal properties include albedo and emissivity values while optical properties include reflectance and transmittance values. On the basis of colour information of point cloud data, reflectance and transmittance values are calculated by referring to a graphics colour taken from the ElumTools library [71], which is also used as a reference for material and artificial lighting simulations in Revit [85]. Reflectance and transmittance values are respectively determined from the following equation.

$$Ref = \left( 0.2125 \frac{R}{255} \right) + \left( 0.7154 \frac{G}{255} \right) + \left( 0.0721 \frac{B}{255} \right) \quad (3)$$

$$Max. Trans = (0.2125 \cdot R_{avail}) + (0.7154 \cdot G_{avail}) + (0.0721 \cdot B_{avail}) \quad (4)$$

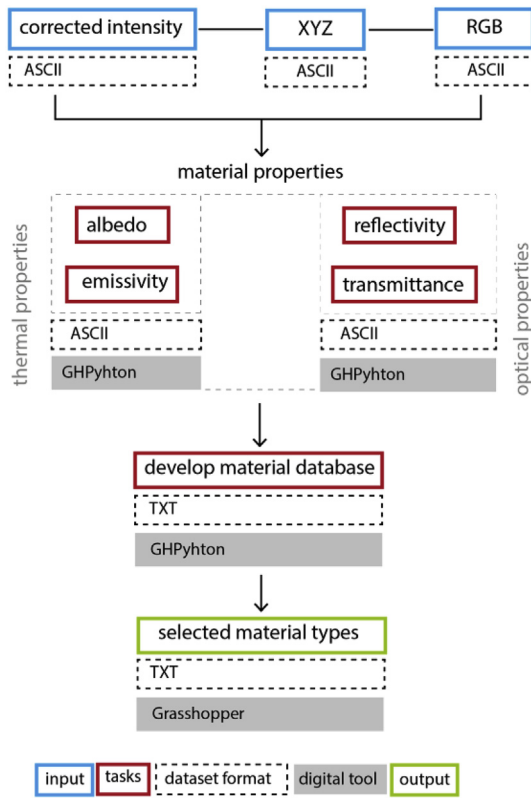


Fig. 3. Material exploration of point cloud data.

$$R_{avail} = R/255 \quad G_{avail} = G/255 \quad B_{avail} = B/255 \quad (5)$$

where Ref = the reflectance value

Max.Trans = maximum transmittance

$R_{avail}$  = the maximum amount of light reflected from the red component

$G_{avail}$  = the maximum amount of light reflected from the green component

$B_{avail}$  = the maximum amount of light reflected from blue component.

To obtain maximum transmittance values, the most heavily reflected component should be initially identified based on non-dichroic transmittance. The resulting component is first subtracted by 1 to find the ratio of transmitted value to reflected light. This ratio is useful as a multiplier in calculating the relative amount of light for the other colour components. Accordingly, maximum transmittance values can be calculated by performing the mathematical operation given in equation (4). Emissivity values are determined from the corrected intensity attributes as both emissivity and intensity based on similar material aspects related to surface reflectance. In this case, however, their values principally work in reverse.

Furthermore, albedo values are computed from both colour information and corrected intensity. As is exemplified in equation (6), the calculation aims at not only measuring light reflected from the average of RGB colours but also capturing incident solar energy through the multiplication of corrected intensity values.

$$Alb = \left( \frac{\sqrt{\left( \frac{R^2 + G^2 + B^2}{3} \right)}}{255} \right) \cdot I_c \quad (6)$$

where Alb = the albedo value

Table 1

Material database for the outdoor building context (collected from various sources).

| Index | Material types                      | Material properties |        |                      |              |
|-------|-------------------------------------|---------------------|--------|----------------------|--------------|
|       |                                     | Emissivity          | Albedo | Reflectance          | Transparency |
| 0     | Brick                               | 0.93                | 0.4    | 0.2                  | Opaque       |
| 1     | Asphalt                             | 0.9                 | 0.12   | 0.07                 | Opaque       |
| 2     | Stone (granite)                     | 0.44                | 0.30   | 0.25                 | Opaque       |
| 3     | Stone (white marble)                | 0.75                | 0.6    | 0.45                 | Opaque       |
| 4     | Wood                                | 0.8                 | 0.35   | 0.5                  | Opaque       |
| 5     | Plaster                             | 0.9                 | 0.4    | 0.65                 | Opaque       |
| 6     | Cement                              | 0.54                | 0.8    | 0.4                  | Opaque       |
| 7     | Ceramic tile                        | 0.5                 | 0.35   | 0.72                 | Opaque       |
| 8     | Glass with a zenith-angle of 40–80° | 0.95                | 0.52   | Transmittance – 0.75 | Translucent  |

R = the red value

G = the green value

B = the blue value

$I_c$  = the corrected intensity value

After establishing formulas for all material properties, each point of a dataset can readily be inputted into the material database. This material database will then evaluate each point in a conditional loop according to the threshold value taken from optical and thermal properties. Due to a lack of compatibility between existing material libraries (e.g., Honeybee-Grasshopper includes Radiance, Open Studio 1.12.0, Energy Plus V8-5-0, THERM 7.6 [86] and CES Edu Pack 2017 [67]) and the proposed method, we propose a sample of relevant materials that matches the conditions of the selected dataset (see Table 1).

Discrepancies between existing material libraries can be observed from computational workflows and materials formats. For example, in Radiance, material setup involves using a specific type of material at the beginning of the workflow, which is then followed by material properties. By contrast, the method proposed in this work involves identifying materials at the end of the workflow as the output according to the selection process used for the point cloud dataset. Considerable efforts have been made to compensate for this issue by inputting material properties in CES Edu Pack beforehand. This approach generates several types of materials that correspond with input properties. However, a further consideration not only concerns the availability of material properties but also the complex range of material types that are to some extent seemingly irrelevant to the proposed context. For example, material selection in CES Edu Pack concludes with formation of many unexpected variations of specific engineering materials. Such a result would produce biased outputs from this study, which is intended to deal with architectural materials used for outdoor building surfaces.

### 3.1.2. Simulation of solar radiation

Due to the requirement of similar inputs from point cloud data (see Fig. 1), the proposed process (stage 2b) is based on a similar level as that of stage 2a focused on material properties. As such, a portion of the employed dataset also takes selected points from the corrected intensity values. The workflow of our simulation of solar radiation is illustrated in Fig. 4.

In general, the simulation of solar radiation involves the use of two main inputs: the sun's direction vector from the environmental variable and normal vectors of the site surfaces. The calculation of the sun vector involves the use of climate and geographic inputs such as latitude, longitude, and the specific point of time of given a year. Specifically, for this study this process is performed by using components available through Grasshopper, some of which include Ladybug and DIVA, but of course this can be done with other tools. Meanwhile, normal vectors of

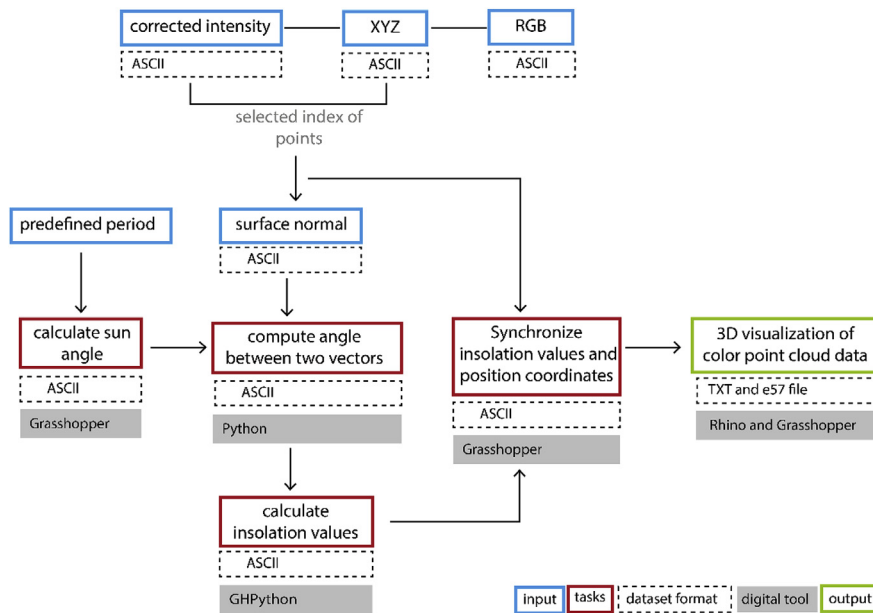


Fig. 4. Solar radiation simulation workflow.

site surfaces are computed in CC due to the large number of points to be calculated.

With a trigonometric principle (see Fig. 5) the insolation values of each point of a dataset can be calculated from the normal irradiance (the angle between sun vectors and normal vectors of the site surfaces) multiplied by the cosine of the angle of incidence (INC). In principle, solar energy is fully absorbed by the surface when the sun vector and the normal vectors are aligned. To reflect this, the cosine value of the angle will be 1 when the angle formed is zero such that as the angle increases, the cosine value will decline.

Furthermore, the following process requires the use of a synchronization value between the simulation result of the insolation analysis and the index of the coordinate position from the initial dataset. This allows for the identification of a surface's degree of direct sun exposure for the point cloud dataset. With a colour 3D point cloud, the lowest and the highest degrees of direct sun exposure can then be visualized to each point of the dataset. For outputs the proposed workflow produces a 3D point cloud model aligned with an ASCII file that presents a simulation analysis of the dataset.

### 3.1.3. Integrated environmental simulation

This stage involves investigating an integrated workflow between a material database and a simulation of solar radiation. It aims to not only identify materials in areas exposed to a certain level of direct

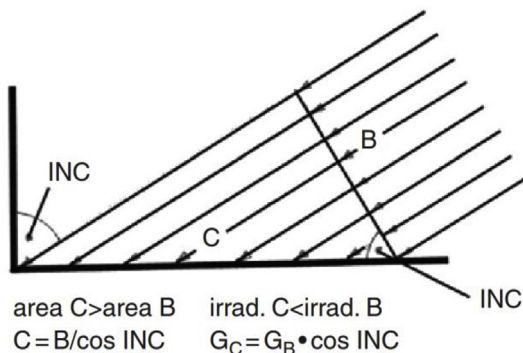


Fig. 5. Calculation of solar irradiance (INC: angle of incidence, G: global irradiance) [87].

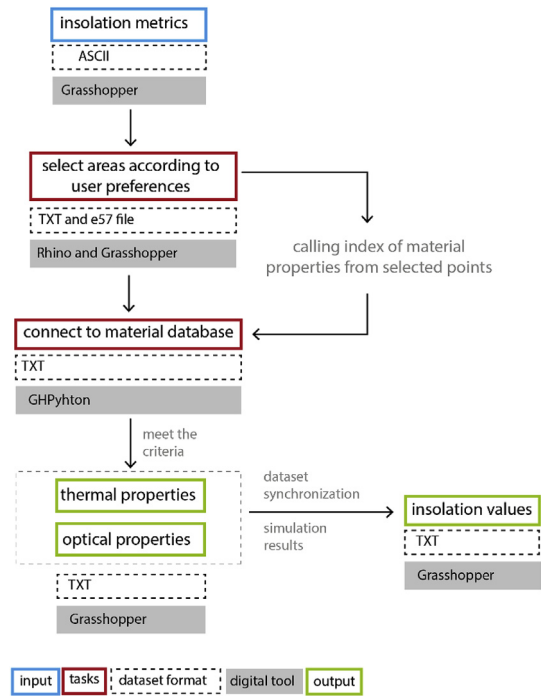


Fig. 6. Simulation of solar radiation.

sunlight but to also generate a highly informed site database through a fully integrated simulation analysis conducted in the preliminary design stage. The following figure describes the process of the integrated workflow (see Fig. 6).

The main procedure of the workflow focuses on material selection according to material properties of the point cloud dataset. In this workflow, insolation values are integrated with material types such that surfaces subjected to high or low levels of solar exposure can be identified and extracted along with their materials. In this case, a numerical index of each point within the dataset plays a crucial role in synchronizing metadata between material properties and solar simulation results.

Ultimately, a list of insolation values corresponding with material



Fig. 7. The selected 3D colour point cloud dataset

types is the final output of the proposed integrated workflow. An evaluation of the whole dataset will generate the number of points that meet and do not meet the criteria of the material database. Accordingly, a comprehensive analysis of the environmental performance of the existing context can be conducted. To implement the proposed computational workflow, a sample 3D colour point cloud dataset is used in the following section.

#### 4. Dataset collection

We applied the approach on a selected small sample of 3D point cloud data (see Fig. 7). Several criteria are used during dataset collection, some of which include the following: *First*, the dataset consists of a 3D colour-point cloud. Colours can help architects not only visualize the representation of real objects in the digital environment but also analyse the appearance of materials and textures during simulation. *Second*, the dataset includes information on at least three typical attributes as mentioned above: XYZ, RGB, and reflection intensity (I). *Third*, the dataset includes multiple site properties for the sake of material property investigation. After setting these criteria, dataset collection can be applied to any architectural context.

The collected dataset is for a Middlestem Church located in Groningen, the Netherlands. Its geometric properties include a building facade, trees and a surrounding landscape with a total number of points spread across 31,5 million points. Via cloud sub-sampling in CC, the minimum distance between two points can be adjusted to limit the density of points. In this case, the dataset is ultimately set at 5 cm, producing roughly 449,267 points from the total collection of points. Dataset collection is supported with a Faro Focus 3D laser scanner set to a wavelength of 950 nm. We also use a Nikon D5300 DSLR camera for the processing of the 3D colour-point cloud.

#### 5. Study findings and discussion

Having established the selected dataset, this section discusses the implementation of the proposed workflow. The analysis results are presented under four categories: intensity correction, the surface distribution of material properties of the dataset, simulation results of the insolation analysis, and material selection for each selected point cloud dataset. These are presented in the chronological order of the proposed workflow described above.

##### 5.1. Intensity correction

During dataset preparation it is important to first calculate the incident angle before determining the corrected intensity ( $I_c$ ). For an unstructured cloud of points, the surface normal of the points is calculated by using a Hough Normals plugin [88] in CC. This condition requires that such a task identifies optimal normal values in the dataset. Several tolerance angles are then simulated into raw intensity values of

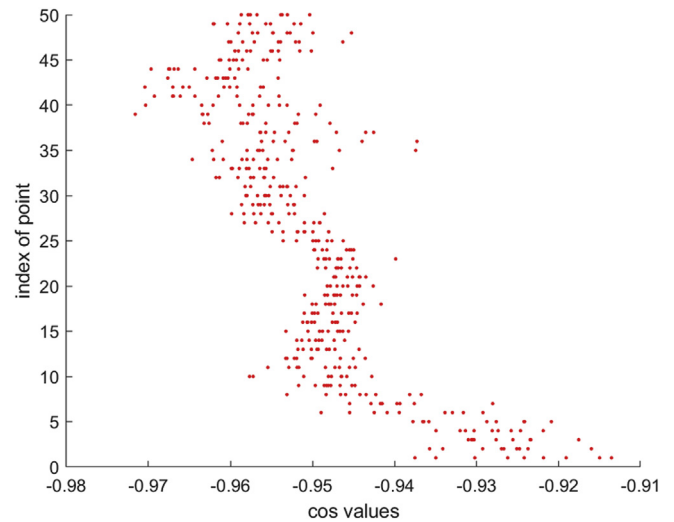


Fig. 8. Distribution of points according to the angle of incidents.

$10^\circ$ – $90^\circ$  (see Fig. 8).

Fig. 8 shows the dispersion of points among cosine values from the range of angles. It shows that points can be scattered at a certain angle. However, the majority of dense points seemingly make up a small portion of each plot of cosine values. It can be said that some points on a certain surface might correspond very well to a laser beam projected at a certain angle during scanning. Roughness and material characteristics of the surface also play an important role in this condition. Furthermore, an evaluation of the scattered points is run by reducing them while maintaining the densest one. In doing so, a standard deviation of each cosine value is plotted to identify the density distribution of points within the dataset (see Fig. 9).

According to the distribution of points shown in Fig. 9, the proximate truncation of the dataset is set to range from 0 to 0.015. What results are roughly 266,864 points or 59.3% of all points. As such, intensity corrections can be calculated using equation (1). Fig. 10 below presents a comparison between the raw dataset and the corrected intensity values.

The following aspects describe major changes in the dataset's performance resulting from the initial intensity level:

- by certain RGB colour features, several geometric properties of the original dataset (specifically trees and edges along the building)

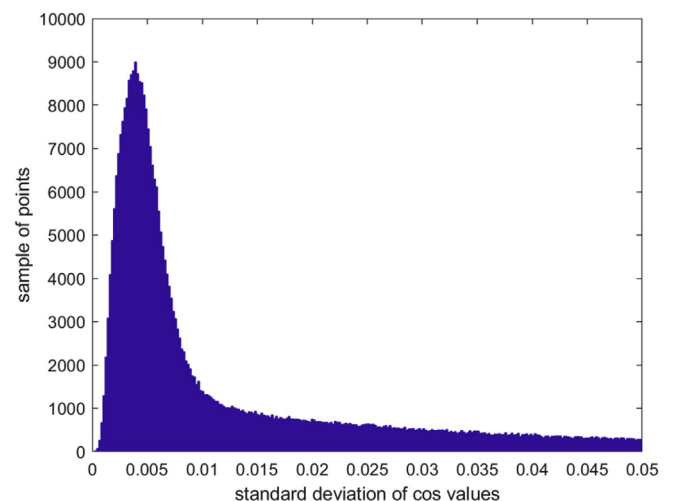


Fig. 9. Distribution of points according to the standard deviations of different cos values.

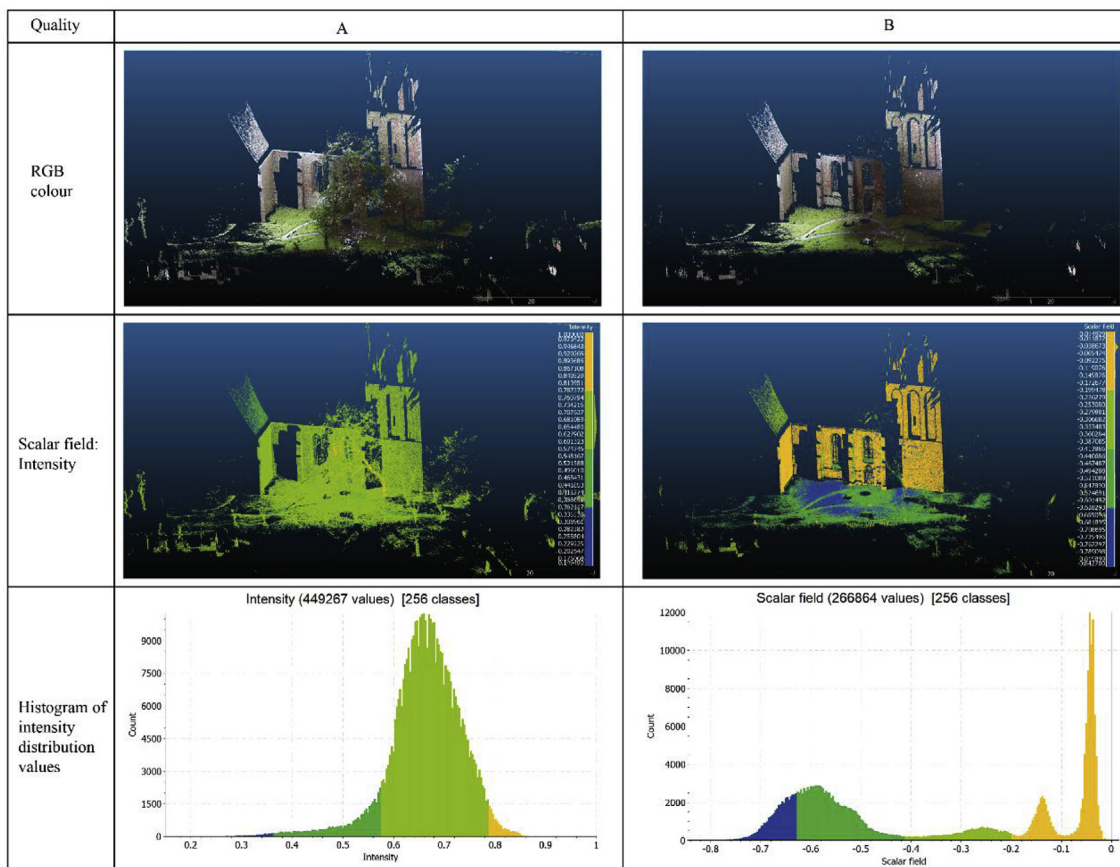


Fig. 10. Comparison of the (A) Original dataset and (B) Corrected intensity.

disappeared. In this case, intensity correction mostly affected not only the scattered points but also the uneven surfaces. This result simultaneously provides us with enough insight to temporarily exclude vegetation properties during the intensity correction phase, as vegetation will considerably affect all dataset values during the calculation of material properties and during the simulation of solar radiation.

- The colour value of intensity also undergoes significant transformation. Four colour steps are set to facilitate the legibility of the intensity range. As a bright colour, the colour yellow represents a high-intensity value that concurrently refers to the most reflective surface while the colour blue denotes the opposite. In Fig. 10-A (see part of the scalar field) the most reflective surfaces are predominantly distributed across the wall of the building. This intensity distribution reveals a major discrepancy from Fig. 10-B based on tree trunks located on reflective surfaces. In general, this serves as a crucial aspect of surface material properties to consider when determining intensity values particularly dealing with real building contexts.
- According to the histogram results, the distribution of intensity values observed within the original dataset concentrates at a green colour representing approximately 89% of the total density of the points. This means that green values are scattered across the entire surface of the dataset. On the other hand, from the calibration of the incident angle of the scanner and the normal vector of the datasets, the corrected intensity values ultimately present an obvious boundary between areas of high (yellow), moderate (green) and low (blue) intensity values.

### 5.2. Surface distribution of material properties

This step involves mapping material properties of the surface of the dataset in parallel with the calculation of point densities of each identified surface. With information on surface materials architects can measure the specific performance of certain areas within an existing dataset. Fig. 11 presents the surface distribution of the selected material properties within a range of 0.0–1.0.

In general, the point density of surface materials follows a similar pattern as property ranges of the largest and smallest values. The three material properties of reflectance, emissivity, and albedo are measured within an equivalent range for the largest values, at 0.0–0.3. These constitute 21.4%, 28.6%, and 21.2% of the total density of points, respectively. The only exceptions found for this largest range are transmittance values, with 19.097% ranging from 0.4 to 0.5. Meanwhile, for the lowest percentages of values, reflectance, emissivity, and transmissivity occupy a similar range of 0.9–1.0. Only the albedo values are valued within a range of 0.0–0.1. Moreover, translucent properties are evaluated by comparing values of average reflectance and transmittance for each point. This evaluation is performed with a Boolean operation. When the reflectance is larger than transmittance values, the translucent material will be *False* and vice versa. The results show that translucent materials constitute 48.7% of the points while the remaining 51.3% have opaque properties. A comparison of these values statistically reveals that surface materials covered within the dataset primarily constitute non-reflective surfaces. This simultaneously shows that other surface characteristics of the existing context mostly include rough textures and high surface temperatures observed during the daytime [89].

A surface material catalogue allows architects to select particular areas to analyse further under an environmental design framework

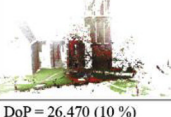
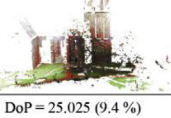
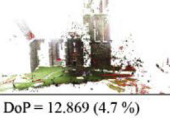
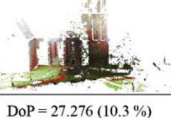
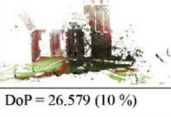
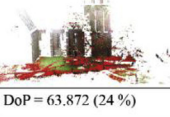
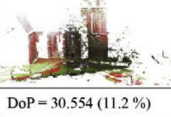
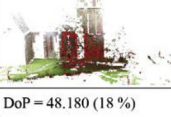
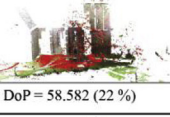
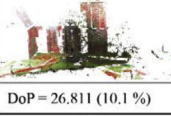
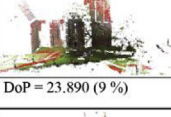
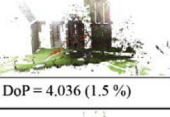
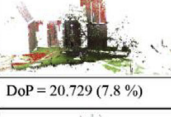
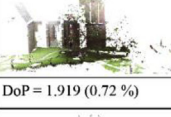
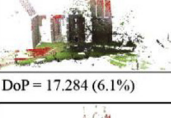
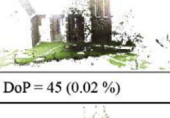
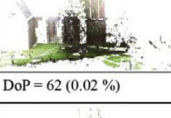
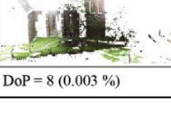
| Threshold values | Average Reflectance  | Emissivity   | Albedo  | Transmissivity   |
|------------------|--|--|---|--|
| 0.0 - 0.1        | <br>DoP = 1.882 (0.7 %)     | <br>DoP = 76.290 (28.6 %) | <br>DoP = 1.600 (0.6 %)     | <br>DoP = 27.657 (10.4 %)   |
| 0.1 - 0.2        | <br>DoP = 44.491 (17 %)     | <br>DoP = 26.755 (10 %)   | <br>DoP = 50.846 (19 %)     | <br>DoP = 37.030 (13.86 %)  |
| 0.2 - 0.3        | <br>DoP = 57.105 (21.4 %)   | <br>DoP = 16.549 (6.18 %) | <br>DoP = 56.534 (21.2 %)   | <br>DoP = 35.411 (13.3 %)   |
| 0.3 - 0.4        | <br>DoP = 26.470 (10 %)     | <br>DoP = 7.885 (3 %)     | <br>DoP = 26.475 (10 %)     | <br>DoP = 44.358 (16.6 %)   |
| 0.4 - 0.5        | <br>DoP = 25.025 (9.4 %)    | <br>DoP = 12.869 (4.7 %)  | <br>DoP = 27.276 (10.3 %)   | <br>DoP = 50.974 (19.097 %) |
| 0.5 - 0.6        | <br>DoP = 26.579 (10 %)    | <br>DoP = 63.872 (24 %)  | <br>DoP = 30.554 (11.2 %)  | <br>DoP = 48.180 (18 %)    |
| 0.6 - 0.7        | <br>DoP = 28.182 (10.4 %) | <br>DoP = 58.582 (22 %) | <br>DoP = 26.811 (10.1 %) | <br>DoP = 21.311 (8 %)    |
| 0.7 - 0.8        | <br>DoP = 23.890 (9 %)    | <br>DoP = 4.036 (1.5 %) | <br>DoP = 20.729 (7.8 %)  | <br>DoP = 1.919 (0.72 %)  |
| 0.8 - 0.9        | <br>DoP = 17.284 (6.1 %)  | <br>DoP = 45 (0.02 %)   | <br>DoP = 12.985 (4.9 %)  | <br>DoP = 62 (0.02 %)     |
| 0.9 - 1.0        | <br>DoP = 15.966 (6 %)    | <br>DoP = 0             | <br>DoP = 12.983 (4.9 %)  | <br>DoP = 8 (0.003 %)     |

Fig. 11. Surface distribution catalogue of material properties.

while providing supplementary information on which design treatments to apply to specific areas based on material parameters.

### 5.3. Simulation of solar radiation

As noted in Section 2.3, this step involves quantifying the solar energy of the existing context according to solar radiation simulation results for a point cloud dataset. In this case, the simulation focuses on the period of June–September 2017 (9 a.m.–8 p.m. Central European

Time) with a coordinate position of 52.1326° N, 5.2913° E. From this setting, 36 values of sun vectors are produced from the sun angle calculation. These vectors are then computed to each surface normal of the point cloud dataset. Accordingly, each point of the dataset is evaluated from 36 sun vectors. The evaluation yields approximately 9.6 million radiation values. The aggregation of the time range will result in robust output values with the effect of consuming time during the simulation process.

Fig. 12 presents simulation results for incoming solar radiation for

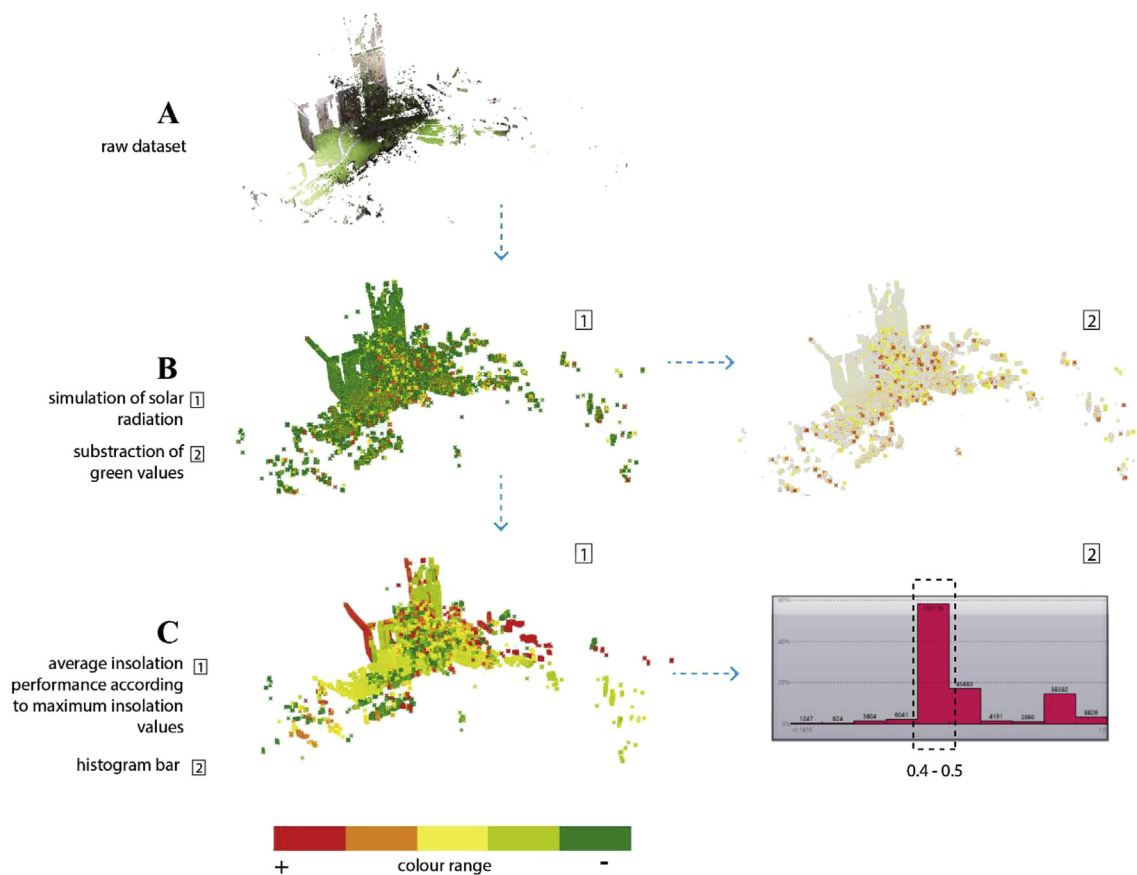


Fig. 12. Simulation of solar radiation.

the point cloud dataset. The simulation results are visualized based on five colour properties ranging from red to green, which respectively denotes high to low radiation values. As is illustrated in Fig. 12-B, less than 10% of all radiation values meet the criteria required to absorb solar energy. The domination of green colours across the surface of the dataset indicates a lack of solar energy absorption. Meanwhile, yellow and red points reflect the dataset remaining from green subtraction (see Fig. 12-B2) and originate from values of 0.8–1.0 according to their histogram bar values.

Fig. 12-C furthermore presents average insolation values received by each point of the dataset. During the simulation, only maximum insolation values from each point are counted. The histogram bar (Fig. 12-C2) shows that yellow colours constitute the largest proportion of insolation values at 0.4–0.5 (58% of all points). On the other hand, red colours as the highest values can only be found in certain areas with low proportion. For example, red points are unevenly distributed along the edges of the building's walls and along tree branches, which are unfortunately less conducive to solar collection technology application.

#### 5.4. Material selection with integrated insolation values

This section discusses the workflow of integration for the material database and for insolation values derived from the simulation of solar radiation. With a developed material database, the proposed algorithm evaluates the material properties of the dataset according to a threshold value of optical or thermal properties. This approach allows for the identification of material types in parallel with the total number of points exhibiting optical or thermal properties. The database is furthermore employed to identify materials presenting certain ranges of insolation values.

According to the material selection results (see Fig. 13), the dataset most likely fulfils the criteria for material properties for the database

(see Table 1). Unknown materials are found those points that do not fulfil the criteria. Eight of the 9 materials successfully meet threshold values for optical properties while for thermal properties only 6 materials meet the selection criteria. Regarding the density of points, the resulting optical properties of the materials are predominantly registered throughout the whole dataset, which includes over 44.9% optical properties. Thermal properties represent only 6.7% of the points.

Further results on this material selection are as follows:

- We find that transmittance criteria heavily affect dataset selection regardless of the number of points of transmittance values. This can be observed, for example, from optical properties, as wood materials quantitatively represent the largest proportion of registered materials, while stone (granite) makes up the lowest proportion. These results can be examined from the material database (see Table 1) and by then referring back to a comparison of surface distribution catalogues (see Fig. 11). In this case, wood and stone (granite) consist of opaque materials with reflectance values of 0.5 and 0.25, respectively. For the range of 0.5, surface distribution values (see Table 1) show that a threshold of 0.5 (0.4–0.6) accounts for over 19% of the density in points in terms of average reflectance. Meanwhile, stone materials (granite) (thresholds of 0.2 to 0.3) account for more points at approximately 21.4%.
- The resulting materials successfully identify a number of points from opaque and translucent materials in terms of both optical and thermal properties.
- The point properties of the dataset confirm similarities among the material types. Accordingly, various objects with different surface characteristics (e.g., roughness and glossiness) can actually be composed of the same materials. This case can be observed from a group of points that fall within several material thresholds. As an example, a point with index 42633 in terms of optical property

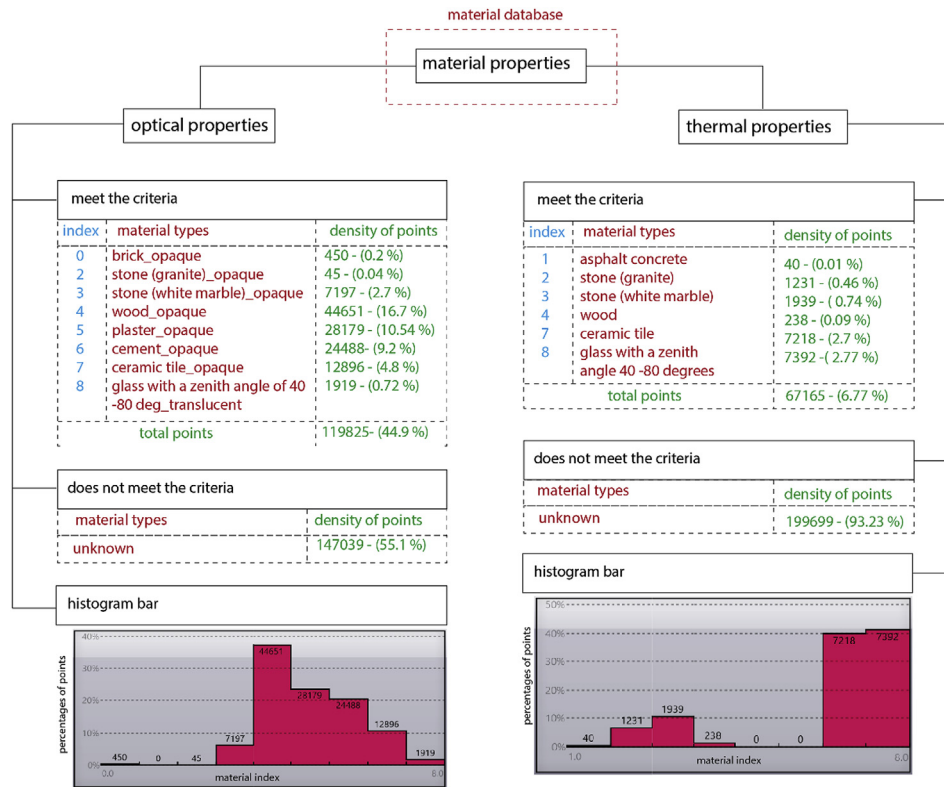


Fig. 13. Material selection according to optical and thermal properties.

criteria refers to three types of materials: stone, wood, and cement. Fleming [90] implicitly confirmed this point in that material estimations computationally support a higher fidelity of representation than mere material categorizations.

The final step of the proposed workflow produces a list of materials found within the dataset according to insolation values generated from the simulation (see Fig. 14). As an input, insolation values of a different colour range (as illustrated in Section 5.3) cover various point densities. From our evaluation of the material database the results show that each colour range on both optical and thermal properties covers a large variety of material types. Eight out of 9 materials were successfully identified for both properties. The properties also follow similar trends in point density for each identified material within the insolation colour range. This result indicates that the developed material database positively responds to calculations of material properties acquired from point clouds of the existing context, highlighting further opportunities to modify the environmental performance of certain areas according to a material analysis.

Fig. 14 shows that the highest material distributions in terms of optical and thermal properties are respectively found for wood (index 4) and glass (index 8), though yellow colours also denote the presence of cement (index 6) in terms of thermal properties. The least common values are found for stone-granite (index 2) in terms of optical properties and for asphalt (index 1) and white stone-marble (index 3) in terms of thermal properties. From the material performance within these properties, environmental characteristics of the context examined in this study can be hypothetically addressed. For example, a massive discrepancy in insolation values between the largest (denoted by light and dark green areas with a point density of over 70%) and smallest portions (denoted by red and orange areas with a point density of only 21%) may affect how the environmental context generates ambient temperature. As Ramirez and Munoz [89] point out, areas absorbing less energy denote high albedo values. It can then be useful to moderate the urban heat island effect. This means that materials within 70%

lower insolation values can be substituted with materials with high albedo values. This strategy may be used to measure the thermal impacts of microclimate issues on the built environment.

## 6. Conclusions and future perspectives

In this study, we perform an environmental performance analysis of an existing context by making use of potential applications of point cloud data. Through material studies and simulations of solar radiation, the proposed computational workflow allows architects to fortify contextual analysis during the initial design stage. Several concluding remarks regarding this process are made as follows:

- The exploration of material properties (optical and thermal) from attribute information on point clouds extends particular functions of 3D scanning technologies related to performance simulation and environmental analysis during the architectural design process. The proposed workflow reveals an additional opportunity to map impacts of the built environment before applying a new building to the selected context.
- Post-processing datasets necessarily help architects not only select relevant information to be employed during analysis but also minimize the environmental effects of dataset measurement during scanning.
- The integrated workflow between the material database and solar simulation may reveal specific characteristics of the existing environment. For example, the identification of highly reflective surfaces or high insolation values of a certain area can help architects to decide whether to maintain or alter the design process.

While the workflow presented in this work presents partially positive results, it requires further consideration in certain respects. For example, dataset corrections may require one to consider more radiometric parameters, especially related to intensity properties such as surface roughness, range, and target reflectance. These parameters are

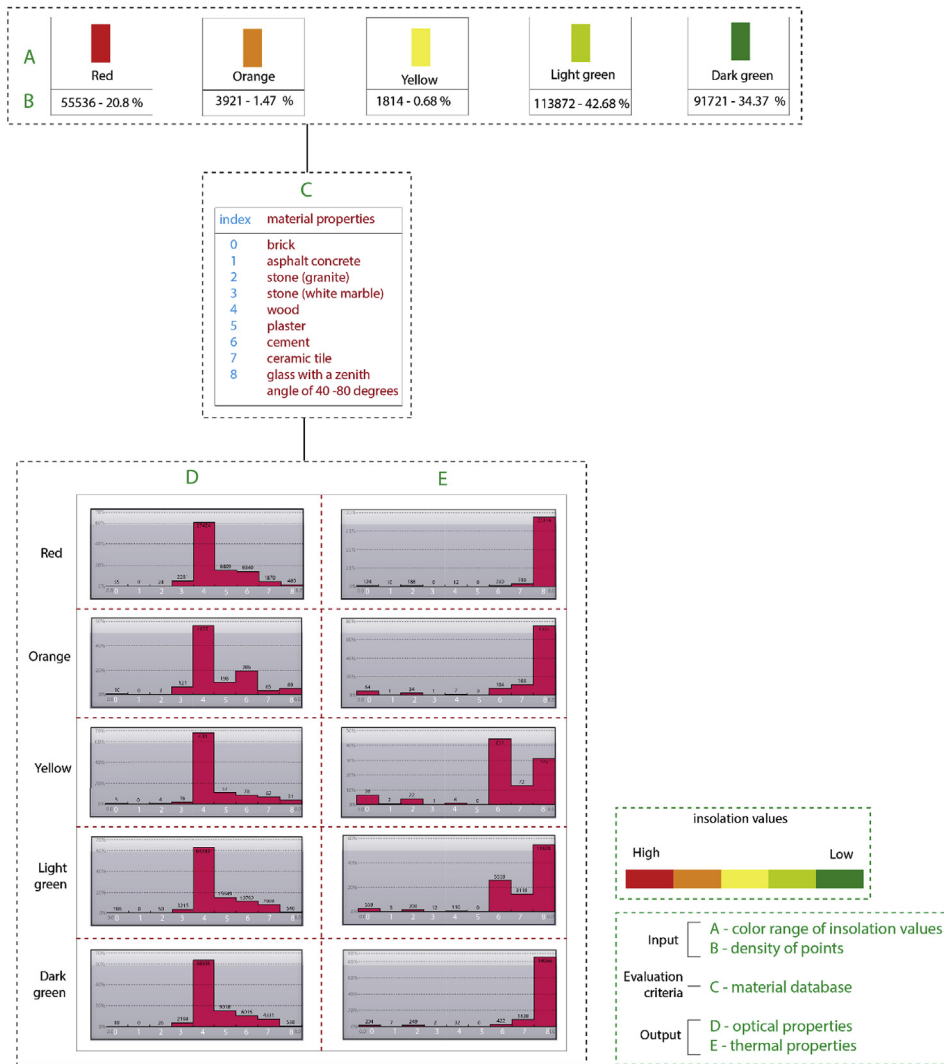


Fig. 14. Material selection according to insolation value simulation results.

expected to reduce erroneous measurements of dataset. Storing more relevant materials in a database also allows for a broad range of selection criteria used for the datasets. The material database employed in this work focuses on demonstrating the feasibility of applying the proposed workflow for architectural design practices.

With further developments from this study may extend several potential features, some of which may include the use of temperature parameters in defining thermal properties to enrich albedo information on existing contexts or expanding the scale of case studies so that aspects of urban morphology and building functions can be addressed. Finally, using a reflectometer in combination with a thermal camera during scanning might prove useful for verifying and calibrating dataset reflectance values.

**Conflict of Interest**

*Declarations of interest*

None.

**Acknowledgements**

This study was financially supported by the Indonesia Endowment Fund for Education (LPDP) as a part of PhD research conducted under the chair of Design Informatics of the Faculty of Architecture and the

Built Environment of TU Delft. The authors would like to express their gratitude to Valentini Vanhecke (4Visualization) for providing access to the dataset used and to Helmiriawan and Yu-Chou Chiang for their technical support during dataset processing.

**References**

- [1] S. Sariyildiz, Conceptual Design by Means of Islamic- Geometric-Patterns within a CAADEnvironment, PhD-thesis Faculty of Architecture, Delft, 1991 TU Delft.
- [2] N.N. Staneva, Approaches for generating 3D solid models in AutoCAD and solid works, J. Eng. VI (3) (2008) 28–31.
- [3] V. Shapiro, "Solid Modeling," Spatial Automation Laboratory, University of Wisconsin, Madison, 2001.
- [4] M.F. Alkadri, M. Turrin, S. Sariyildiz, Identifying the surface materials of the existing environment through point cloud data attributes, SimAUD (Simulation for Architecture and Urban Design), Delft, 2018.
- [5] Y. Arayici, A. Hamilton, P. Gamito, Modelling 3D scanned data to visualize and analyse the built environment for regeneration, Surveying and Built Environment 17 (2) (2006) 7–28.
- [6] Y. Arayici, Towards building information modelling for existing structures, Struct. Surv. 26 (3) (2008) 210–222.
- [7] I. Yüksek, T.T. Karadayi, Energy-efficient building design in the context of building life cycle, Sustainable Development, IntechOpen, London, 2017, pp. 93–123.
- [8] M.F. Alkadri, M. Turrin, S. Sariyildiz, The use and potential applications of point clouds in simulation of solar radiation for solar access in urban contexts, Advances in Computational Design 3 (4) (2018) 319–338.
- [9] L. Bragança, S.M. Vieira, J.B. Andrade, Early stage design decisions: the way to achieve sustainable buildings at lower costs, Sci. World J. 2014 (2014) 1–8.
- [10] T. Kotnik, M. Weinstock, Material, form and force, Architect. Des 82 (2) (2012) 104–111.

- [11] S. Kaasalainen, A.K.A. Krooks, H. Kaartinen, Radiometric calibration of terrestrial laser scanners with external reference targets, *Rem. Sens.* 1 (3) (2009) 144–158.
- [12] A.G. Kashani, M.J. Olsen, C. Parrish, N. Wilson, Review of LIDAR radiometric processing: from ad hoc intensity correction to rigorous radiometric calibration, *Sensors* 15 (11) (2015) 28099–28128.
- [13] D.A. White, LIDAR, point clouds, and their archaeological applications, *Mapping Archaeological Landscapes from Space*, Springer-Verlag New York, New York, 2013, pp. 175–186.
- [14] N.-J. Shih, The application of A 3d scanner in the representation of building construction site, *International Association for Automation and Robotics in Construction, IAARC*, Madrid, 2002.
- [15] T. Várady, R.R. Martin, J. Cox, Reverse engineering of geometric models—an introduction, *Comput. Aided Des.* 29 (4) (1997) 255–268.
- [16] Y. Fujita, I. Kobayashi, W. Chanseawrassamee, F. Hoshino, Application of attributed road surface point cloud data in road maintenance, *Journal of Japan Society of Civil Engineers, Ser. F3 (Civil Engineering Informatics)* 70 (2) (2014) 1185–1192.
- [17] E. Lin, C. Girot, Point cloud components tools for the representation of large scale landscape architectural projects, *Digital Landscape Architecture*, Zurich, 2014.
- [18] E. Lin, K. Shaad, C. Girot, Developing river rehabilitation scenarios by integrating landscape and hydrodynamic modeling for the Ciliwung River in Jakarta, *Indonesia, Sustainable cities and society* 20 (2016) 180–198.
- [19] T.P. Kersten, F. Keller, J. Saenger, J. Schiewe, Automated generation of an historic 4D city model of hamburg and its visualization with the GE engine, *Progress in Cultural Heritage, 4th International Conference, EuroMed, 2012Limassol*, 2012.
- [20] M. Balzani, C. Bughi, F. Ferrari, L. Rossato, A. Tursi, Alberti's box: the cultural multimedia project on the architectures of Leon Battista Alberti, *Progress in Cultural Heritage Preservation, 4th International Conference, EuroMed, 2012Limassol*, 2012.
- [21] W. Moussa, M. Abdel-Wahab, D. Frisch, Automatic fusion of digital images and laser scanner data for heritage preservation, *Progress in Cultural Heritage Preservation, 4th International Conference, EuroMed, 2012Limassol*, 2012.
- [22] L. Bornaz, A. Lingua, F. Rinaudo, Engineering and environmental applications of laser scanner techniques, *ISPRS Commission III Symposium " Photogrammetric Computer Vision"*, Graz, 2002.
- [23] R. Kassner, W. Koppe, T. Schüttenberg, G. Bareth, Analysis of the solar potential of roofs by using official lidar data, *ISPRS Congress Beijing, Beijing*, 2008.
- [24] C. Carneiro, E. Morello, G. Desthieux, Assessment of solar irradiance on the urban fabric for the production of renewable energy using LIDAR data and image processing techniques, *Advances in GIScience, Hannover*, 2009.
- [25] M. Weinmann, *Reconstruction and Analysis of 3D Scenes*, Springer International Publishing, Karlsruhe, 2016.
- [26] J. Otepka, S. Ghuffar, C. Waldhauser, R. Hochreiter, N. Pfeifer, Georeferenced point clouds: a survey of features and point cloud management, *ISPRS Int. J. Geo-Inf.* 2 (4) (2013) 2038–2065.
- [27] T. Randall, *Client Guide to 3D Scanning and Data Capture*, BIM Task Group, UK, 2013.
- [28] A. Gressin, C. Mallet, J. Demantké, N. David, Towards 3D lidar point cloud registration improvement using optimal neighborhood knowledge, *ISPRS J. Photogrammetry Remote Sens.* 79 (2013) 240–251.
- [29] V. Salehi, S. Wang, Using point cloud technology for process simulation in the context of digital factory based on a system engineering integrated approach, *The 21st International Conference on Engineering Design, ICED 17*, Vancouver, 2017.
- [30] D. Sidiropoulou-Velidou, A. Georgopoulos, J.L. Lerma, Exploitation of thermal imagery for the detection of pathologies in monuments, *Progress in Cultural Heritage Preservation, 4th International Conference, EuroMed, 2012Limassol*, 2012.
- [31] E. Gigliarelli, D. Carlea, A. Corcella, H. Porfyriou, Historical social housing: smart analysis and design for conservation and energy conservation, *Progress in Cultural Heritage Preservation, 4th International Conference, EuroMed, 2012Limassol*, 2012.
- [32] R. Richter, J. Döllner, Concepts and techniques for integration, analysis and visualization of massive 3D point clouds, *Comput. Environ. Urban Syst.* 45 (2014) 114–124.
- [33] I. Kobayashi, Y. Fujita, H. Sugihara, K. Yamamoto, Attribute analysis of point cloud data with color information, *Journal of Japan Society of Civil Engineers* 67 (2) (2011) 95–102.
- [34] B. Höfle, M. Hollaus, J. Hagenauer, Urban vegetation detection using radiometrically calibrated smallfootprint full-waveform airborne LiDAR data, *ISPRS J. Photogrammetry Remote Sens.* 67 (2012) 134–147.
- [35] A. Brzank, C. Heipke, J. Goepfert, U. Soergel, Aspects of generating precise digital terrain models in the Wadden Sea from lidar–water classification and structure line extraction, *ISPRS J. Photogrammetry Remote Sens.* 63 (5) (2008) 510–528.
- [36] N.J. Mitra, A. Nguyen, L. Guibas, Estimating surface normals in noisy point cloud data, *Int. J. Comput. Geom. Appl.* 14 (2004) 261–276.
- [37] Q.-Y. Zhou, U. Neumann, Fast and extensible building modeling from airborne LiDAR data, *Proceedings of the 16th ACM SIGSPATIAL International Conference on Advances in Geographic Information Systems, Irvine*, 2008.
- [38] K.-H. Bae, D.D. Lichti, A method for automated registration of unorganised point clouds, *ISPRS J. Photogrammetry Remote Sens.* 63 (1) (2008) 36–54.
- [39] Y. Fujita, Y. Hoshino, S. Ogata, I. Kobayashi, Attribute assignment to point cloud data and its usage, *Glob. J. Comput. Sci. Technol.* 15 (2) (2015) 2–B.
- [40] Y. Fujita, I. Kobayashi, Y. Hoshino, W. Chanseawrassamee, Development of attribute-assign-editor for road surface point cloud data, *IACSIT International Journal of Engineering and Technology* 8 (3) (2016) 170–176.
- [41] E. Lin, Y. Ninsalam, M.F. Prescott, Augmenting XYZRGB: design and the reality captured landscape, *Kerb Journal of Landscape Architecture* 23 (2015) 112–113.
- [42] S. Ochmann, R. Vock, R. Wessel, R. Klein, Automatic reconstruction of parametric building models from indoor point clouds, *Comput. Graph.* 54 (2016) 94–103.
- [43] ArcMap, **What is lidar intensity data?** Available: <http://desktop.arcgis.com/en/arcmap/10.3/manage-data/las-dataset/what-is-intensity-data-htm>, (2016) , Accessed date: 7 December 2018.
- [44] T. Voegtle, I.R. Schwab, T. Landes, Influences of different materials on the measurements of a terrestrial laser scanner (tls), *Int. Arch. Photogramm. Remote Sens. Spat. Inf. Sci.* 37 (5) (2008) 1061–1066.
- [45] C. Suchocki, W. Błaszczyk-Bak, Down-sampling of point clouds for the technical diagnostics of buildings and structures, *Geosciences* 9 (2) (2019) 1–14.
- [46] J. Armesto-González, B. Riveiro-Rodríguez, D. González-Aguilera, M.T. Rivas-Brea, Terrestrial laser scanning intensity data applied to damage detection for historical buildings, *J. Archaeol. Sci.* 37 (12) (2010) 3037–3047.
- [47] S.S. Soudarissanane, *The Geometry of Terrestrial Laser Scanning*, PhD-thesis Faculty of Civil Engineering and Geoscience, TU Delft, Delft, 2016.
- [48] A.-B. Mostafa, M. Ebrahim, 3D laser scanners' techniques overview, *Int. J. Sci. Res.* 4 (10) (2015) 323–331.
- [49] S. Crutchley, Using LiDAR in archaeological contexts: the English heritage experience and lessons learned, *Laser Scanning for the Environmental Sciences*, Wiley-Blackwell, West Sussex, 2009, pp. 180–200.
- [50] S. Sasidharan, A normalization scheme for terrestrial LiDAR intensity data by range and incidence angle, *International Journal of Emerging Technology and Advanced Engineering* 6 (5) (2016) 322–328.
- [51] R. Blaskow, D. Schneider, Analysis and correction of the dependency between laser scanner intensity values and range, *The International Archives of the Photogrammetry, ISPRS Technical Commission V Symposium, Riva del Garda*, 2014.
- [52] K. Tan, X. Cheng, Correction of incidence angle and distance effects on TLS intensity data based on reference targets, *Rem. Sens.* 8 (3) (2016) 251.
- [53] S. Kaasalainen, A. Jaakkola, M. Kaasalainen, A. Krooks, A. Kukko, Analysis of incidence angle and distance effects on terrestrial laser scanner intensity: search for correction methods, *Rem. Sens.* 3 (10) (2011) 2207–2221.
- [54] D. Constantino, M.G. Angelini, Qualitative and quantitative evaluation of the luminance of laser scanner radiation for the classification of materials, *Int. Arch. Photogramm. Remote Sens. Spatial Inf. Sci., XL-5/W2*, Strasbourg, 2013.
- [55] D. Lichti, B. Harvey, The effects of reflecting surface material properties on time-of-flight laser scanner measurements, *Symposium on Geospatial Theory, Processing and Applications*, Ottawa, 2002.
- [56] Y. Reshetuk, Investigation of the influence of surface reflectance on the measurements with the terrestrial laser scanner leica HDS 3000, *Zeitschrift für Geodäsie, Geoinformation und Landmanagement* 131 (2) (2006) 96–103.
- [57] M.U. Hassan, A. Akcamete-Gungor, C. Meral, Investigation of terrestrial laser scanning reflectance intensity and RGB distributions to assist construction material identification, *The Joint Conference on Computing in Construction (JC3)*, Heraklion, 2017.
- [58] T. Voegtle, I.R. Schwab, T. Landes, Influences of different materials on the measurement of a terrestrial laser scanner ( TLS ), *Proceedings of the XXI ISPRS Congress, the International Archives of the Photogrammetry, Remote Sensing and Spatial Information Sciences, Beijing*, 2008.
- [59] X. Li, Y. Liang, Surface characteristics modeling and performance evaluation of urban building materials using LIDAR data, *Appl. Optic.* 54 (15) (2015) 4750–4759.
- [60] B.B. Worstell, S.K. Poppenga, G.A. Evans, S.A. Prince, *Lidar Point Density Analysis- Implications for Identifying Water Bodies*, Rolla Publishing Service Center, Sioux Falls, 2014.
- [61] G. Kigle-Boeckler, Measurement of gloss and reflection properties of surfaces, *Met. Finish.* 93 (5) (1965) 28–31.
- [62] N. Alam, *SlideShare*, " 18 6, (2014) Available: <https://www.slideshare.net/NajmaAlam/thermal-properties-of-materials> , Accessed date: 15 November 2017.
- [63] E. Dobos, Albedo, *Encyclopedia of Soil Science*, CRC Press, Boca Raton, 2006, pp. 64–66.
- [64] J. Coackley, Reflectance and albedo, surface, *Encyclopedia of the Atmosphere*, Oregon State University, Corvallis, 2003, pp. 1914–1923.
- [65] M. Councils, *Whiter than White*, Creative Materials Consultant Limited, London, 2012.
- [66] H. Taha, D. Sailor, H. Akbari, High-Albedo Materials for Reducing Building Cooling Energy Use, *California Institute for Energy Efficiency (CIEE)*, Berkeley, 1992.
- [67] M. Ashby, J. Fernandez, A. Gray, *Granta Education Hub*, (2008) Available: <https://teachingresources.grantadesign.com/Edition/Architecture/PAPARCEN06> , Accessed date: 14 May 2018.
- [68] NTC-TTP, *New Technologies Research Centre*, (2000) Available: <https://ttp.zcu.cz/en/laboratories/optical-properties/optical-properties/emissivity> , Accessed date: 1 May 2018.
- [69] *Optotherm, Optotherm Thermal Imaging*, (2018) Available: <https://www.optotherm.com/emiss-examples.htm> , Accessed date: 5 May 2018.
- [70] A. Marsh, *Performative Design*, (2010) Available: <http://performativedesign.com/definition/light-reflectivity/> , Accessed date: 5 May 2018.
- [71] *ElumTools, Elumtools*, (2012) Available: <http://www.elumtools.com/docs/2012/Content/Using%20ElumTools/Color%20Reflectance%20or%20Transmittance.htm> , Accessed date: 6 May 2018.
- [72] D. Nagy, *Generative Design*, (27 2 2017) Available: <https://medium.com/generative-design/solar-analysis-in-grasshopper-5dae76c9b6cb> , Accessed date: 7 September 2018.
- [73] M.F. Alkadri, M. Turrin, S. Sariyildiz, The use and potential applications of point clouds in simulation of solar radiation for solar access in urban contexts, *Advances in Computational Design* 3 (4) (2018) 319–338.
- [74] M. Horvat, M.-C. Dubois, Tools and methods for solar design—an overview of IEA SHC task 41, subtask B, *1st International Conference on Solar Heating and*

- Coolingfor Buildings and Industry (SHC 2012), San Fransisco, 2012.
- [75] N. Lukač, D. Žlaus, S. Seme, B. Žalik, G. Štumberger, Rating of roofs' surfaces regarding their solar potential and suitability for PV systems, based on LiDAR data, *Appl. Energy* 102 (2012) 803–812.
- [76] A. Jochem, V. Wichmann, B. Höfle, Large areas point cloud based solar radiation modeling, *Hamburger Beiträge zur Physischen Geographie und Landschaftsökologie*, 2010, pp. 1–9.
- [77] J. Liang, J. Gong, W. Li, A.N. Ibrahim, A visualization-oriented 3D method for efficient computation of urban solar radiation based on 3D-2D surface mapping, *Int. J. Geogr. Inf. Sci.* 28 (4) (2014) 780–798.
- [78] A. Jochem, B. Höfle, M. Rutzinger, Extraction of vertical walls from mobile laser scanning data for solar potential assessment, *Rem. Sens.* 3 (4) (2011) 650–667.
- [79] A. Pavlovski, J. Fletcher, V. Kostylev, J. Crace, Solar architecture and energy engineering, *Journal of Green Building* 5 (2) (2010) 32–40.
- [80] Y. Li, D. Ding, C. Liu, C. Wang, A pixel-based approach to estimation of solar energy potential on building roofs, *Energy Build.* 129 (2016) 563–567.
- [81] M.E. Charlton, S.J. Coveney, T. McCarthy, Issues in laser scanning, *Laser Scanning for the Environmental Sciences*, Wiley-Blackwell, West Sussex, 2009, pp. 35–48.
- [82] S.D. Bartolo, R. Salvini, Multitemporal terrestrial laser scanning for marble extraction assessment in an underground quarry of the apuan alps (Italy), *Sensors* 19 (3) (2019) 1–10.
- [83] M.N. Favorskaya, L.C. Jain, *Handbook on Advances in Remote Sensing and Geographic Information Systems*, Springer International Publishing AG, Cham, 2017.
- [84] D. Girardeau-Montaut, *Cloud-Compare*, (2015) Available: <http://www.cloudcompare.org/doc/qCC/CloudCompare%20v2.6.1%20-%20User%20manual.pdf> , Accessed date: 5 February 2018.
- [85] A. Goyal, *Lmn Architects*, " 29 10 2014, Available: <https://lmnarchitects.com/tech-studio/bim/revit-daylighting-tools-2-elumtools/> , Accessed date: 1 April 2018.
- [86] M.S. Roudsari, P. Michelle, *Ladybug: a Parametric Environmental Plugin for Grasshopper to Help Designers Create an Environmentally-Conscious Design*, Lyon, (2013).
- [87] S.V. Szokolay, *Introduction to Architectural Science: : the Basis of Sustainable Design*, Elsevier/Architectural Press, Oxford, 2008.
- [88] A. Boulch, R. Marlet, *Deep learning for robust normal estimation in unstructured point clouds*, *Eurographics Symposium on Geometry Processing*, Berlin, 2016.
- [89] A.Z. Ramirez, C.B. Muñoz, *Albedo effect and energy efficiency of cities, Sustainable Development - Energy, Engineering and Technologies - Manufacturing and Environment*, Intech, Rijeka, 2012, pp. 1–18.
- [90] R.W. Fleming, *Visual perception of materials and their properties*, *Vis. Res.* 94 (2013) 62–75.